Finite-temperature calculation of the isovector giant dipole resonance in ^{120}Sn using self-consistent inputs

Sujan Kumar Roy ⬤, Chandrani Sen ⬤, Supriya Mukhopadhyay, and Jhilam Sadhukhan
Physics Group, Variable Energy Cyclotron Centre, Kolkata 700064, India
and Homi Bhabha National Institute, Mumbai 400094, India

Background: Although microscopic models are frequently used to investigate giant resonances built on the ground state of a nucleus, similar calculations at nonzero temperature are limited. Approaches based on the classical thermal shape-fluctuation model (TSFM) are often utilized to analyze the properties of giant dipole resonance at finite temperature. However, TSFM fails to predict the correct trend of resonance width over a wide range of temperature starting from zero.

Purpose: To study the isovector giant dipole resonance (IVGDR) at finite temperature, we present an improved version of TSFM, where driving potential and IVGDR centroid energies are obtained self-consistently using the nuclear energy density functional formalism. The temperature dependence of IVGDR width in ^{120}Sn is calculated to benchmark the proposed method.

Method: Nuclear free energy surfaces and entropy surfaces are simulated at different temperatures for two different parametrizations of Skyrme energy density functionals. Moreover, IVGDR centroid energies are calculated by incorporating nuclear deformations extracted from the corresponding self-consistent densities. Subsequently, IVGDR widths are obtained within TSFM. Also, we demonstrate the role of pairing fluctuation in improving the low temperature behavior of IVGDR width.

Result: We found good overall agreement of our results with the measured IVGDR widths. Specifically, except at a very low temperature, unprecedented accuracy has been achieved in TSFM. Calculated IVGDR widths are shown to be robust against the choices of driving potential and Skyrme parametrization.

Conclusion: The present paper provides guidance on using TSFM based calculations in predicting the IVGDR width over a broad range of temperature. For a more consistent calculation, pairing fluctuations are required to be included as additional degrees of freedom.

I. INTRODUCTION

The width of isovector giant dipole resonance (IVGDR) is an important observable to understand the structural details of excited nuclei [1,2]. Over the last several decades, numerous experiments have been performed [3–11] to extract the behavior of IVGDR width as a function of nuclear angular momentum and temperature. In parallel, various theoretical models have been proposed to explain these dependencies. However, a comprehensive theoretical understanding of this process is still missing as the associated collective dynamics is strongly correlated to the underlying motion of individual nucleons. The scenario becomes even more complicated when IVGDR appears on an excited state with nonzero angular momentum and/or temperature.

The response from collective vibrations in nuclei can be calculated microscopically by employing different variants of the random phase approximation (RPA) [12–17] and quasiparticle RPA (QRPA) [18–21]. Nuclear dipole oscillations can also be simulated by using a more general dynamical framework as adopted within the time-dependent density functional theory (TDDFT) [22–25]. To study IVGDR built

on excited states, a method based on finite-temperature QRPA (FT-QRPA) [26] is applied. However, FT-QRPA fails to reproduce the experimental IVGDR widths due to lack of proper accounting of the collective excitation [27]. Also, a relativistic version of finite-temperature mean-field theory was proposed [28,29], but it exhibits a sharper temperature dependence in the IVGDR width compared to the measured values [29,30]. The experimental temperature dependence of IVGDR width can be traced with the phonon damping model (PDM) [31–34]. In this model, phonon energies and their coupling with single-particle states are adjusted to match the ground-state IVGDR width. Then, finite-temperature behavior is extracted for fixed values of these parameters.

Alternatively, the thermal shape fluctuation model (TSFM) [35–39] can be used to get the IVGDR response from thermally excited nuclei. In TSFM, nuclei are considered to populate different configurations (shapes) following thermal equilibrium. Further, the collective motion is assumed to obey the adiabaticity condition [40,41]. Helmholtz's free energy is generally used in TSFM to determine the probability of different configurations [42–45]. In current implementations of TSFM, free energy surfaces (FESs) are obtained within the

Nilsson-Strutinsky approach [35,40,46,47], where the configuration space is restricted to quadrupole moments defined by the shape coordinates β and γ [48]. Also, IVGDR centroid energies are calculated assuming exact ellipsoidal shapes. The standard description of TSFM thus obtained cannot reproduce the observed temperature dependence of IVGDR width [49], especially at temperatures $\leqslant 2$ MeV. Although improvement in TSFM was attempted [37,50] through consistent calculation of the IVGDR response function and the associated FES, observed enhancement in the IVGDR width was not enough to match the measured temperature and angular momentum dependences. In a separate work [46], incorporation of pairing fluctuations in TSFM was found to be an efficient way to reproduce the low-temperature behavior of IVGDR width.

In this paper, we demonstrate that a more reliable prediction of the temperature dependence of IVGDR width can be achieved when the FES in TSFM is calculated from the finite-temperature density functional theory (FT-DFT) and, simultaneously, the IVGDR centroid energies are corrected for the corresponding energy-optimizing shapes. These shapes may not be necessarily ellipsoidal even though only quadrupole moments are constrained during the self-consistent calculation. We also show that our results remain insensitive to the choice of energy density functional parametrization and to the thermodynamic potential out of two different possibilities: FES and the constant-energy entropy surface (ES).

The theoretical framework used in the present work is elaborated in Sec. II. Subsequently, calculated results are explained in Sec. III. Finally, we conclude in Sec. IV.

II. THEORETICAL FRAMEWORK

We employ β and γ as independent constraints for the FT-DFT calculation. Hence, the expectation value of an observable $\mathcal{O}$ is given by [51]

$$\langle \mathcal{O} \rangle = \frac{\int_\beta \int_\gamma D[\beta, \gamma] P(\beta, \gamma) \mathcal{O}}{\int_\beta \int_\gamma D[\beta, \gamma] P(\beta, \gamma)}, \quad (1)$$

where $D[\beta, \gamma] \equiv \beta^4 |\sin 3\gamma| d\beta d\gamma$ and $P(\beta, \gamma)$ represents the relative probability of a particular shape (β, γ) with respect to the spherical configuration $(\beta = 0, \gamma = 0)$. For a canonical ensemble of thermally equilibrated nuclei at temperature T,

$$P(\beta, \gamma) \equiv P_F(\beta, \gamma; T) \propto \exp\left(-\frac{F(\beta, \gamma; T) - F_0}{T}\right), \quad (2)$$

where $F(\beta, \gamma; T)$ describes the FES and $F_0 \equiv F(0, 0; T)$. The total energy E of an isolated nucleus remains constant during the collective oscillations and, hence, P can be expressed more appropriately as [52]

$$P(\beta, \gamma) \equiv P_S(\beta, \gamma; E) \propto \exp\left(S(\beta, \gamma; E) - S_0\right), \quad (3)$$

where $S(\beta, \gamma; E)$ portrays the ES for a particular E and $S_0 \equiv S(0, 0; E)$.

A. Free energy and entropy from FT-DFT

We calculate the potential energy surface by solving the finite-temperature Hartree-Fock-Bogoliubov (FT-HFB) formalism [53–55] where the total energy E_{HFB} is obtained

self-consistently from the constrained Routhian [56],

$$\hat{H}' = \hat{H}_{HFB} - \sum_{\mu=0,2} \lambda_\mu \hat{Q}_{2\mu} - \sum_{\tau=n,p} \lambda_\tau \hat{N}_\tau. \quad (4)$$

Here, $\hat{H}_{HFB}$ represents the FT-HFB Hamiltonian. $\hat{N}_\tau$ are neutron ($\tau = n$) and proton ($\tau = p$) particle-number operators with λ_τ being the associated chemical potentials. $\hat{Q}_{2\mu}$ are the axial ($\mu = 0$) and nonaxial ($\mu = 2$) components of the mass quadrupole moment operator, and these are uniquely related [48] to β and γ. In general, FT-HFB equations can be written as a nonlinear eigenvalue problem [57]:

$$\begin{pmatrix} h' & \Delta \\ -\Delta^* & -h'^* \end{pmatrix} \begin{pmatrix} U & V^* \\ V & U^* \end{pmatrix} = \begin{pmatrix} U & V^* \\ V & U^* \end{pmatrix} \begin{pmatrix} E & 0 \\ 0 & -E \end{pmatrix}, \quad (5)$$

where U and V are matrices defining quasiparticle states, and E is a diagonal matrix of quasiparticle energies E_k. The single-particle Routhian $h'[\rho]$ and the pairing field $\Delta[\kappa]$ are obtained by minimizing $\hat{H}'$ with respect to the particle (ρ) and pairing (κ) densities. At finite temperature [53,58],

$$\rho = U f U^\dagger + V^* (1 - f) V^T,$$
$$\kappa = U f V^\dagger + V^* (1 - f) U^T, \quad (6)$$

where f is a diagonal matrix such that $f_{ik} = \delta_{ik} f_k$ with

$$f_k = \frac{1}{1 + e^{E_k/k_B T}}. \quad (7)$$

After solving Eq. 5, E_{HFB} can be obtained from the statistical average:

$$E_{HFB} = \langle \hat{H}_{HFB} \rangle = Tr(\hat{D} \hat{H}_{HFB}), \quad (8)$$

where the density operator $\hat{D}$ for the FT-HFB system is given by [53]

$$\hat{D} = \prod_k [f_k \hat{n}_k + (1 - f_k)(1 - \hat{n}_k)]. \quad (9)$$

The quasiparticle number operators, $\hat{n}_k$s are obtained from the U and V matrices. For a particular deformation (β, γ), entropy S can be calculated as [53],

$$S = -k_B \sum_k [f_k \ln f_k + (1 - f_k) \ln(1 - f_k)]. \quad (10)$$

Subsequently, the FES required in Eq. (2) is extracted by employing the thermodynamics relation

$$F = E_{HFB} - ST. \quad (11)$$

For Eq. (3), we need to calculate entropy for a fixed E_{HFB}. This is achieved by interpolating S out of different FESs.

Two different Skyrme parametrizations, namely SkM* [59] and Sly4 [60], are used in h'. For Δ, we employ the zero-range density-dependent mixed pairing interaction given by [61,62]

$$\Delta(\boldsymbol{r}) = \tfrac{1}{2} f(\boldsymbol{r}) \kappa(\boldsymbol{r}) \quad (12)$$

with

$$f(\boldsymbol{r}) = V_0^\tau \left[1 - \frac{1}{2} \frac{\rho(\boldsymbol{r})}{\rho_0}\right], \quad (13)$$

where ρ_0 is the saturation density 0.16 fm^{-3}. The neutron pairing strength V_0^n is locally adjusted to reproduce the isotopic

three-point odd-even mass difference in ^{120}Sn. The same value is taken for V_0^p. We further use different combinations of V_0^n and V_0^p for a qualitative understanding of the role of pairing fluctuations. The symmetry unrestricted DFT solver HFODD (v2.49t) [63] is used for the present self-consistent calculation.

B. IVGDR strength function from self-consistent densities

In case of IVGDR vibration, $\mathcal{O}$ in Eq. (1) is the IVGDR strength function $\mathcal{F}$, which can be expressed as a function of the γ-ray energy E_γ by using the Breit-Wigner formula [2,64]:

$$\mathcal{F}(E_\gamma) = \sum_{\{x_i\}} \mathcal{F}_{x_i} = C_n \frac{NZ}{A} \sum_{\{x_i\}} \frac{(E_\gamma \Gamma_{x_i})^2}{\left(E_\gamma^2 - E_{x_i}^2\right)^2 + (E_\gamma \Gamma_{x_i})^2}.$$
(14)

Here, N, Z, and A are the neutron number, atomic number, and mass number of the nucleus, respectively, and C_n is a normalization constant determined by the sum rule [65]. In Eq. (14), sum is taken over the components ($\mathcal{F}_{x_i}$) of $\mathcal{F}$ along the three body-fixed principal axes x_i, $i = 1, 2, 3$. E_{x_i} and Γ_{x_i} are the centroid energy and FWHM of $\mathcal{F}_{x_i}$, respectively. These quantities obey the empirical relations [2,66]

$$E_{x_i} = E_0\left(\frac{R_0}{R_{x_i}}\right) \quad \text{and} \quad \Gamma_{x_i} = \Gamma_0\left(\frac{R_0}{R_{x_i}}\right)^{1.6}, \quad (15)$$

where $E_0 = 18.0A^{-1/3} + 25.0A^{-1/6}$ and $\Gamma_0 = 3.64$ MeV are the values of E_{x_i} and Γ_{x_i}, respectively, for the spherical shape with radius R_0. For ellipsoidal shapes [67],

$$R_{x_i} = R_0 \exp\left[\sqrt{\frac{5}{4\pi}}\beta\cos\left(\gamma - \frac{2\pi}{3}i\right)\right]. \quad (16)$$

This definition of R_{x_i} is usually used in the macroscopic-microscopic (mac-mic) versions of TSFM where nuclear shapes are restricted to quadrupole moments generated by the geometrical shape parameters β and γ. However, deformations arising from the self-consistent calculation may differ from an exact ellipsoidal shape. To account for this, we propose to modify Eq. (16) as

$$R_{x_i} = R_0 \exp\left[\frac{x_i^{\text{rms}} - x_{i0}^{\text{rms}}}{x_{i0}^{\text{rms}}}\right], \quad (17)$$

where $x_i^{\text{rms}} \equiv \sqrt{\langle x_i^2 \rangle}$ and x_{i0}^{rms} is the value of x_i^{rms} for the spherical shape. x_i^{rms}s incorporate the effects due to self-consistent density distribution. With Eq. (17), we have verified that the volume conservation condition $R_{x_1}R_{x_2}R_{x_3} = R_0^3$ is hardly violated even at the highest T considered. Maximum deviation in the nuclear volume is $\approx 4\%$ and it occurs at a very large β where the relative probability P is <0.01.

We calculate the canonical [Eq. (2)] and microcanonical [Eq. (3)] averages of $\mathcal{F}$, yielding the average GDR widths Γ_F' and Γ_E', respectively. In case of Γ_E', the E axis is transformed to the T axis by employing the Fermi gas formula $T = \sqrt{E/a}$, a being the level density parameter, which is assumed to be $A/9$ in the present work.

C. Contribution from particle evaporation

At higher temperature (for $T \geqslant 2$ MeV in general), IVGDR width is further broadened [40,68,69] due to evaporation of light particles and statistical γ rays. As we have verified for the present system, a major contribution in this respect comes only from evaporation of neutrons. Moreover, evaporation may occur either from the initial state or from a state after the GDR decay. Therefore, we need to account for the enhancement in GDR width considering both the possibilities [70]. Consequently, the total GDR width will be $\Gamma_{F,E} = \Gamma_{F,E}' + 2\Gamma_{\text{CN}}$ [71], where Γ_{CN} is the sum of particle (neutron, proton, and α) and γ evaporation widths of the compound nucleus. We neglect the variation in Γ_{CN} caused by the GDR decay. All the widths in Γ_{CN} are calculated from the statistical prescription described in [72].

III. RESULTS

We consider the IVGDR width of ^{120}Sn to benchmark our model since the measured data [5,6] for this system are available over a wide range of temperature. We moreover select particular measurements where angular momentum effects are negligible as the corrections due to nuclear angular momentum are not included in the present model.

A. Inputs for IVGDR width calculation

Figure 1 illustrates FESs and ESs of ^{120}Sn obtained with the Sly4 EDFs at different T and E ($\equiv E_{HFB}$), respectively. Below $T = 1$ MeV, behavior of FES is strongly influenced by the pairing interaction [54]. Hence, FES does not change much at $T = 0.5$ MeV. Then, FES flattens out as T increases considerably and it effectively leads to a broadening of the IVGDR width. For ES, the accessible (β, γ) space is limited by the fixed-E criterion and, as depicted in Fig. 1, the allowed region grows as E increases. Also, entropy changes with deformation in a similar manner as the free energy; i.e., for large E, ES becomes smooth enough to populate large deformations following P_S. We have checked that FESs and ESs from SkM* also show a pattern similar to Sly4.

To asses the impact of R_{x_i} as prescribed in Eq. (17), we define a quantity r_{x_i}, which is the ratio of R_{x_i} in Eq. (17) to the Hill-Wheeler semiaxes given in Eq. (16). Variations of r_{x_i} for each x_i are plotted in Fig. 2. Here, x_3 represents the symmetry axis for prolate deformation. It is evident that self-consistent shapes deviate from an ellipsoidal configuration at large deformations. Specifically, $r_{x_3} < 1$ for large β and small γ, which indicates the preference for a more compact shape than ellipsoid. Moreover, for deformations with large β and γ, self-consistent calculation enhances triaxiality by stretching the density along the longer semiminor axis x_1. As a result, $r_{x_1} > 1$ while $r_{x_2} \approx 1$ at theses extreme deformations. To understand the structural details more precisely, we extract the hexadecapole moment (Q_{40}) from self-consistent densities. The landscape of Q_{40} on the (β, γ) plane is shown in Fig. 2. Although the absolute magnitude of Q_{40} is small everywhere, Q_{40} is relatively large in the region where nuclear shape deviates considerably from an ellipsoid.
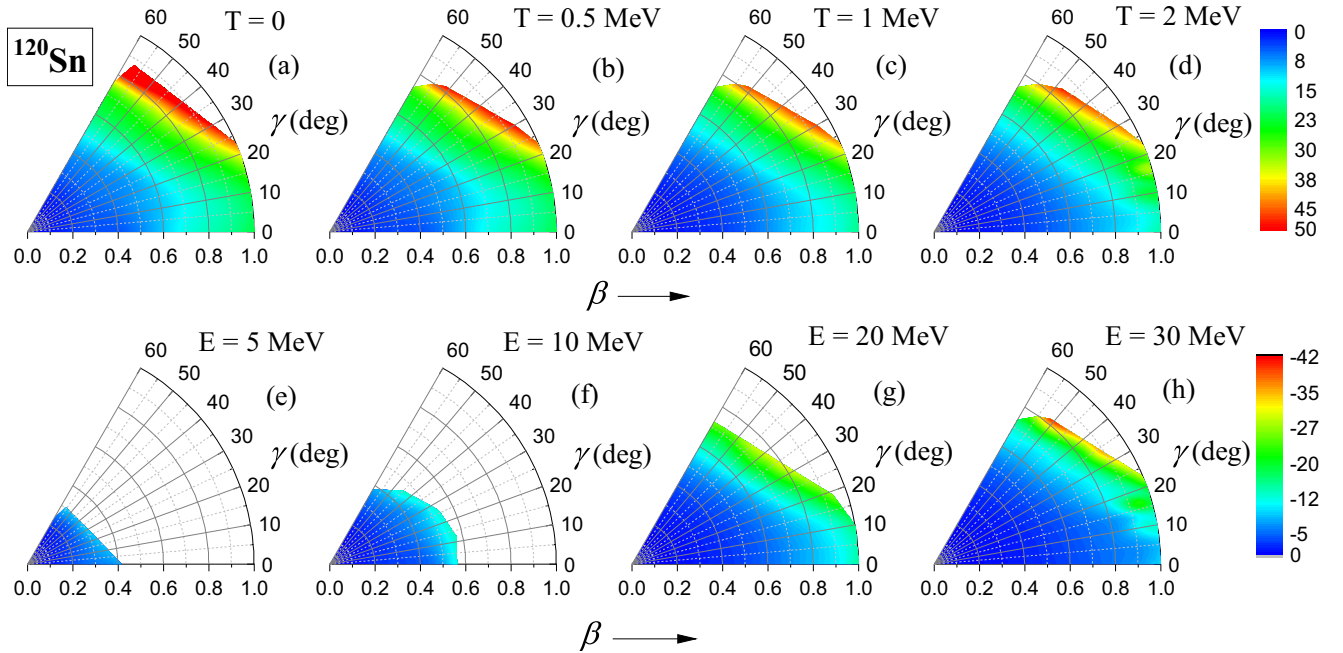
FIG. 1. (a)–(d) Free energy surfaces $[F(\beta, \gamma; T) - F_0]$ for ^{120}Sn calculated for Sly4 EDFs at different T as indicated. (e)–(h) Constant energy entropy surfaces $[S(\beta, \gamma; E) - S_0]$ from Sly4 EDFs.

The IVGDR strength functions ($\mathcal{F}$) arising form the two different prescriptions of R_{x_i} [Eq. (16) and Eq. (17)] are compared in Fig. 3 for various combinations of β and γ. As β increases, $\mathcal{F}$ becomes broader with distinct resonance peaks appearing at the respective centroid energies. In contrast, this broadening is somewhat inhibited when the modified form of R_{x_i} in Eq. (17) is used. It is in accordance with the shape dependence of r_{x_i} as demonstrated in Fig. 1.
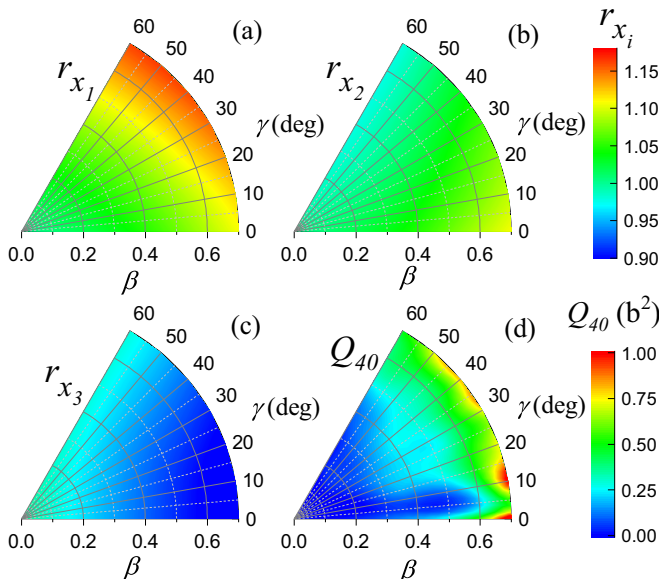
B. Comparison of IVGDR widths from different inputs

The robustness of our results against both the categories of driving potential and EDF parametrizations is tested in Fig. 4. It shows that, apart from small deviations around $T = 1$ MeV, Γ_E almost coincides with Γ_F for both SkM* and Sly4 interactions. We could not calculate Γ_E below a certain T because of computational restrictions: the FT-DFT calculation must to be performed in a finer (β, γ) mesh to generate a large enough number of points below $E = 5$ MeV. The overlap between Γ_F and Γ_E reaffirms [45,52] the applicability of
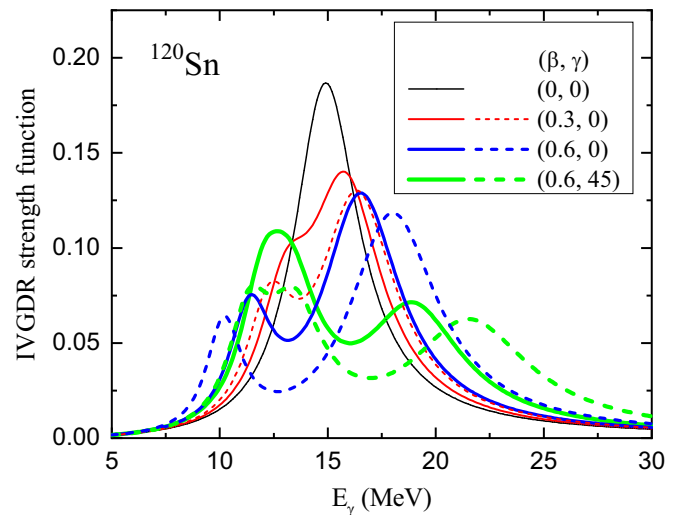

FIG. 2. (a)–(c) Variations of r_{x_i}s on the (β, γ) plane calculated for ^{120}Sn with SkM* EDFs. (d) Corresponding variation of Q_{40}.

FIG. 3. IVGDR strength function corresponding to various combinations of β and γ. Solid and dashed lines are obtained with R_{x_i} in Eqs. (17) and (16), respectively.
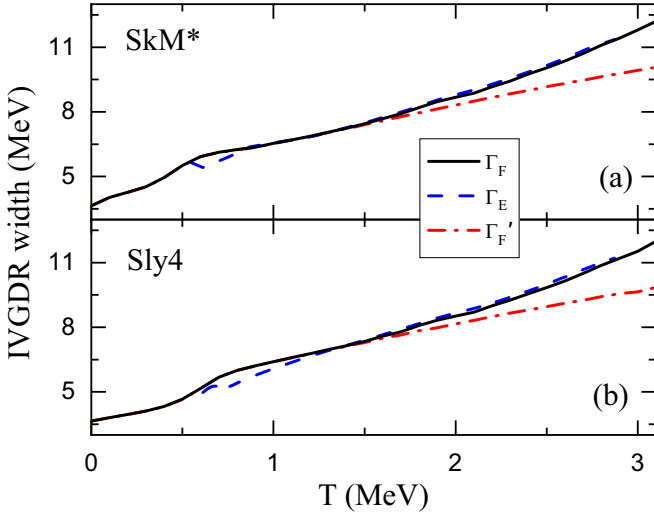
FIG. 4. (a) Total IVGDR width (including particle evaporation width Γ_p) calculated for SkM* EDFs from canonical (solid line) and microcanonical (dashed line) averaging of the IVGDR strength function. The dash dotted line is the canonical average without Γ_{CN}. (b) Same quantities calculated for Sly4 EDFs.

canonical thermodynamics in TSFM. Also, Fig. 4 indicates that our results are independent of the choice of EDFs. For both EDF variants, the IVGDR width approaches saturation at $T \approx 3$ MeV unless we account for the enhancement due to Γ_{CN}. Here, the contribution from Γ_{CN} is of similar magnitude to that reported in [71]. A small bump in IVGDR width appears in $0.5 \leqslant T \leqslant 1$ MeV because of a sharp change in the potential profile in this region.

In Fig. 5, we display a detailed comparison of our prediction with the IVGDR width from existing theoretical models.
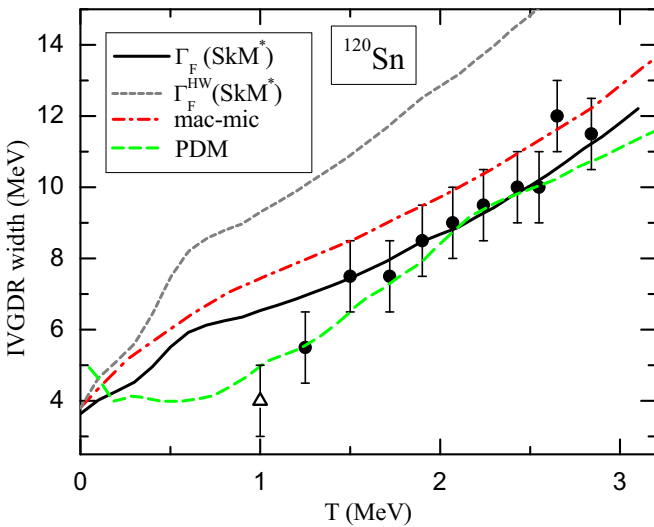

FIG. 5. IVGDR width from present calculations (solid and thin dashed lines) are compared with results (thick dashed and dash dotted lines) from PDM [73] (thick dashed line) and mac-mic [36] (dash dotted line). Experimental widths are indicated by circles [74] and triangle [6].

To this end, we consider two popular models: (i) the TSFM based on the mac-mic inputs [36] and (ii) the PDM that includes appropriate pairing interaction [73]. Mac-mic results are further augmented with the particle evaporation width to maintain consistency with our calculation. Since the calculated widths are almost independent of the chosen EDF parametrizations and the type of driving potential, we arbitrarily select the Γ_F from SkM* parametrization to compare in Fig. 5. Also, we include the IVGDR width Γ_F^{HW}, where Hill-Wheeler radii [Eq. (16)] are used instead of the R_{x_i}'s proposed in Eq. (17). Except at 1 MeV, the rest of the experimental data are taken from Ref. [74]. We further reanalyze the data to extract the average temperature at each data point. To this end, we follow the procedure introduced in [70]. Here, a lower cut in the excitation energy is determined in such a way that the IVGDR decay seizes below this energy. A more detailed description of this method can be found in [11,75].

As is evident in Fig. 5, Γ_F^{HW} drastically overpredicts the measured data over the whole range of T. It clearly indicates the inconsistency in assuming pure ellipsoidal shapes while using self-consistent frameworks for other inputs. In contrast, good overall agreement is achieved when IVGDR centroid energies are properly obtained from the associated self-consistent density distributions. Further, as illustrated in Fig. 5, the measured trend of IVGDR width as a function of T could be reproduced more accurately by our model in comparison to the predictions from the mac-mic based TSFM, which grossly overestimate the data when evaporation widths are added. Although PDM provides a superior T dependence in the low T region where paring fluctuations play a crucial role, the agreement with our predictions is marginally better in the mid-T region: $1.5 \leqslant T \leqslant 2$ MeV.

C. Effect of pairing fluctuation

We extended the present study to understand the possible effects of pairing fluctuations on the IVGDR width below $T = 1$ MeV. The ominant role of pairing fluctuations in ^{120}Sn was demonstrated in [47], where pairing gaps for neutrons (Δ_n) and protons (Δ_p) were treated as independent coordinates. It was shown that, for both Δ_n and Δ_p, an average pairing gap of $\gtrsim 1$ MeV is required to reproduce the experimental data up to $T = 2$ MeV. Also, the extracted $\langle \Delta_n \rangle$ and $\langle \Delta_p \rangle$ [averages taken over the (β, γ) space] vary smoothly within this range of temperature. In contrast, the pairing gap from self-consistent calculations usually quenches at a much lower temperature, $T \approx 1$ MeV.

In current implementations of the HFB formalism, average values of Δ_n and Δ_p are determined self-consistently and these cannot be used directly as free parameters. To this end, as proposed in [56], dynamical paring gaps can be probed by constraining the HFB Hamiltonian with the particle number fluctuations. However, implementation of such a method is beyond the scope of the present work as it involves large-scale simulation on a multidimensional hyperspace. Alternatively, we adjust the pairing strengths V_0^τ to assess the effect of pairing fluctuations. As representative cases, we consider three combinations of V_0^n and V_0^p: (i) $V_0^n = -253.40$ MeV and $V_0^p = -253.40$ MeV, where V_0^n reproduces the experimental
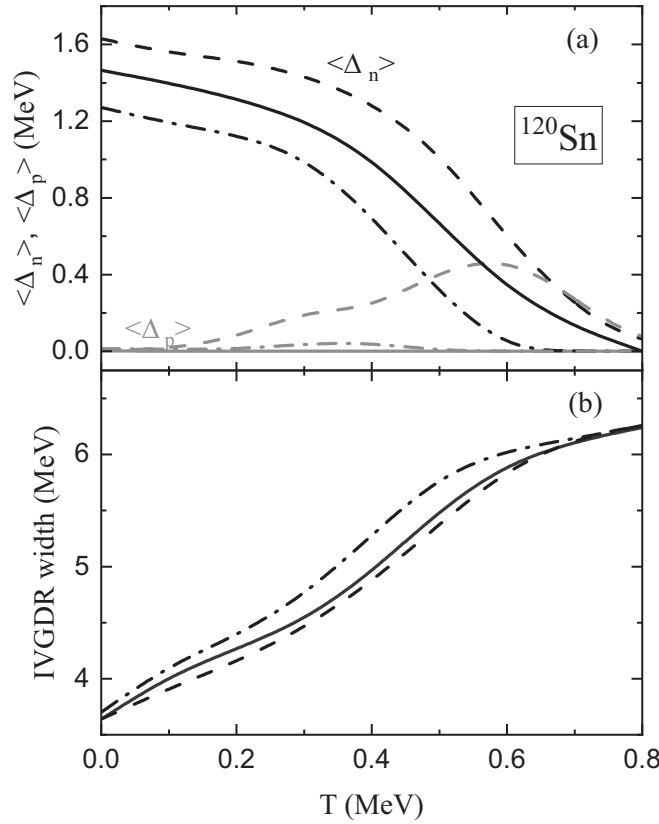
FIG. 6. (a) Temperature dependence of average pairing gaps $\langle \Delta_n \rangle$ (black lines) and $\langle \Delta_p \rangle$ (grey lines) calculated for V_0^n and V_0^p combinations (i) (solid lines), (ii) (dashed lines), and (iii) (dash-dotted lines) as defined in the text. The average is taken over the (β, γ) space. (b) Corresponding IVGDR widths.

ground-state neutron pairing gap (these values are also used for calculations above); (ii) $V_0^n = -265.25$ MeV and $V_0^p = -340.06$ MeV, which are frequently used for heavy nuclei

[76]; and (iii) $V_0^n = -240$ MeV and $V_0^p = -300$ MeV, an arbitrary choice that reduces the overall pairing gap. Although this limited number of choices do not exhaust the whole (Δ_n, Δ_p) space, they can provide a qualitative understanding of the correlation between pairing fluctuation and IVGDR width.

The calculated $\langle \Delta_n \rangle$ and $\langle \Delta_p \rangle$ for (i), (ii), and (iii) are plotted in Fig. 6 as a function of T. Evidently, except for (ii), $\langle \Delta_p \rangle$ remains almost zero for the full T range. This is consistent with the existing result [47] for the closed-proton-shell nucleus ^{120}Sn. Also, $\langle \Delta_p \rangle$ from (ii) indicates the necessity for an even stronger V_0^p to produce a reasonable pairing gap in protons: the experimental ground-state Δ_p from the three-point formula is 2.46 MeV. As Fig. 6 shows, $\langle \Delta_n \rangle$ changes monotonically with V_0^n. Corresponding IVGDR widths are also plotted in Fig. 6 and, as expected, a larger pairing gap suppresses the IVGDR width. However, the overall shift in the width is small due to the restricted variation in $\langle \Delta_\tau \rangle$. A proper thermodynamic averaging over the whole (Δ_n, Δ_p) space may improve the result. Further, as $\langle \Delta_n \rangle$ disappears, all three IVGDR widths merge with a decreasing slope. It depicts a correlation between the nuclear paring and IVGDR width.

IV. CONCLUSION

We presented an improved version of TSFM, where microscopic DFT inputs are implemented to calculate the IVGDR width of ^{120}Sn. Our model is found to be quite insensitive to the theoretical parameters like the choice of interaction and thermodynamic potential. Our results show better agreement with the experimental data in comparison to the conventional mac-mic predictions. The low-temperature behavior of IVGDR width depends strongly on the nuclear paring and, in addition to the standard static paring; we need to incorporate pairing fluctuations [47] to achieve a better agreement in this region. We qualitatively explain the plausible effect of pairing fluctuations. More comprehensive study along this direction is in progress.

[1] K. A. Snover, Giant resonances in excited nuclei, Annu. Rev. Nucl. Part. Sci. **36**, 545 (1986).

[2] J. J. Gaardhoje, Nuclear structure at high excitation energy studied with giant resonances, Annu. Rev. Nucl. Part. Sci. **42**, 483 (1992).

[3] A. Bracco, J. J. Gaardhøje, A. M. Bruce, J. D. Garrett, B. Herskind, M. Pignanelli, D. Barnéoud, H. Nifenecker, J. A. Pinston, C. Ristori, F. Schussler, J. Bacelar, and H. Hofmann, Saturation of the Width of the Giant Dipole Resonance at High Temperature, Phys. Rev. Lett. **62**, 2080 (1989).

[4] M. Kicińska-Habior, K. A. Snover, J. A. Behr, C. A. Gossett, J. H. Gundlach, and G. Feldman, Comparison of giant dipole resonance decay in stiff ^{92}Mo and soft ^{100}Mo excited nuclei, Phys. Rev. C **45**, 569 (1992).

[5] T. Baumann, E. Ramakrishnan, A. Azhari, J. Beene, R. Charity, J. Dempsey, M. Halbert, P.-F. Hua, R. Kryger, P. Mueller, R. Pfaff, D. Sarantites, L. Sobotka, D. Stracener, M. Thoennessen,

G. Van Buren, R. Varner, and S. Yokoyama, Evolution of the giant dipole resonance in excited ^{120}Sn and ^{208}Pb nuclei populated by inelastic alpha scattering, Nucl. Phys. A **635**, 428 (1998).

[6] P. Heckman, D. Bazin, J. Beene, Y. Blumenfeld, M. Chromik, M. Halbert, J. Liang, E. Mohrmann, T. Nakamura, A. Navin, B. Sherrill, K. Snover, M. Thoennessen, E. Tryggestad, and R. Varner, Low-temperature measurement of the giant dipole resonance width, Phys. Lett. B **555**, 43 (2003).

[7] D. Pandit, S. Mukhopadhyay, S. Bhattacharya, S. Pal, A. De, S. Bhattacharya, C. Bhattacharya, K. Banerjee, S. Kundu, T. K. Rana, A. Dey, G. Mukherjee, T. Ghosh, D. Gupta, and S. R. Banerjee, Extreme nuclear shapes examined via giant dipole resonance lineshapes in hot light-mass systems, Phys. Rev. C **81**, 061302(R) (2010).

[8] D. R. Chakrabarty, V. M. Datar, S. Kumar, G. Mishra, E. T. Mirgule, A. Mitra, P. C. Rout, V. Nanal, D. Pandit, S. Mukhopadhyay, and S. Bhattacharya, Exclusive giant

dipole resonance measurement on the Jacobi transition in the ^{19}F$+^{27}$Al system, Phys. Rev. C **85**, 044619 (2012).

[9] S. Mukhopadhyay, D. Pandit, S. Pal, S. Bhattacharya, A. De, S. Bhattacharya, C. Bhattacharya, K. Banerjee, S. Kundu, T. Rana, G. Mukherjee, R. Pandey, M. Gohil, H. Pai, J. Meena, and S. Banerjee, Measurement of giant dipole resonance width at low temperature: A new experimental perspective, Phys. Lett. B **709**, 9 (2012).

[10] M. Ciemała, M. Kmiecik, A. Maj, K. Mazurek, A. Bracco, V. L. Kravchuk, G. Casini, S. Barlini, G. Baiocco, L. Bardelli, P. Bednarczyk, G. Benzoni, M. Bini, N. Blasi, S. Brambilla, M. Bruno, F. Camera, S. Carboni, M. Cinausero, A. Chbihi *et al.*, Giant dipole resonance built on hot rotating nuclei produced during evaporation of light particles from the ^{88}Mo compound nucleus, Phys. Rev. C **91**, 054313 (2015).

[11] S. Mukhopadhyay, P. Roy, D. Mondal, D. Pandit, S. Pal, B. Dey, S. Bhattacharya, A. De, T. K. Rana, S. Kundu, J. Sadhukhan, C. Bhattacharya, and S. R. Banerjee, No signature of the saturation of giant dipole resonance width in medium-mass nuclei, Phys. Rev. C **104**, L031304 (2021).

[12] K. Goeke and J. Speth, Theory of giant resonances, Annu. Rev. Nucl. Part. Sci. **32**, 65 (1982).

[13] K.-F. Liu, H. Luo, Z. Ma, and Q. Shen, Skyrme-landau parameterization of effective interactions: (II). Self-consistent description of giant multipole resonances, Nucl. Phys. A **534**, 25 (1991).

[14] S. Shlomo and G. Bertsch, Nuclear response in the continuum, Nucl. Phys. A **243**, 507 (1975).

[15] T. Sil, S. Shlomo, B. K. Agrawal, and P.-G. Reinhard, Effects of self-consistency violation in Hartree-Fock RPA calculations for nuclear giant resonances revisited, Phys. Rev. C **73**, 034316 (2006).

[16] P. Ring and J. Speth, RPA-calculations in ^{208}Pb with a density dependent interaction, Phys. Lett. B **44**, 477 (1973).

[17] H. Sagawa and G. Bertsch, Self-consistent calculations of finite temperature nuclear response function, Phys. Lett. B **146**, 138 (1984).

[18] S. Péru and H. Goutte, Role of deformation on giant resonances within the quasiparticle random-phase approximation and the gogny force, Phys. Rev. C **77**, 044313 (2008).

[19] K. Yoshida and N. V. Giai, Low-lying dipole resonance in neutron-rich Ne isotopes, Phys. Rev. C **78**, 014305 (2008).

[20] K. Hagino, N. Van Giai, and H. Sagawa, Continuum QRPA response for deformed neutron-rich nuclei, Nucl. Phys. A **731**, 264 (2004).

[21] T. Oishi, M. Kortelainen, and N. Hinohara, Finite amplitude method applied to the giant dipole resonance in heavy rare-earth nuclei, Phys. Rev. C **93**, 034329 (2016).

[22] T. Nakatsukasa and K. Yabana, Linear response theory in the continuum for deformed nuclei: Green's function vs time-dependent Hartree-Fock with the absorbing boundary condition, Phys. Rev. C **71**, 024301 (2005).

[23] C. Simenel and P. Chomaz, Nonlinear vibrations in nuclei, Phys. Rev. C **68**, 024302 (2003).

[24] Y. Shi, N. Hinohara, and B. Schuetrumpf, Implementation of nuclear time-dependent density-functional theory and its application to the nuclear isovector electric dipole resonance, Phys. Rev. C **102**, 044325 (2020).

[25] J. Maruhn, P.-G. Reinhard, P. Stevenson, and A. Umar, The TDHF code Sky3D, Comput. Phys. Commun. **185**, 2195 (2014).

[26] E. Yüksel, G. Colò, E. Khan, Y. F. Niu, and K. Bozkurt, Multipole excitations in hot nuclei within the finite temperature quasiparticle random phase approximation framework, Phys. Rev. C **96**, 024303 (2017).

[27] D. R. Chakrabarty, N. Dinh Dang, and V. M. Datar, Giant dipole resonance in hot rotating nuclei, Eur. Phys. J. A **52**, 143 (2016).

[28] Y. K. Gambhir, J. P. Maharana, G. A. Lalazissis, C. P. Panos, and P. Ring, Temperature dependent relativistic mean field for highly excited hot nuclei, Phys. Rev. C **62**, 054610 (2000).

[29] E. Litvinova and H. Wibowo, Nuclear response in a finite-temperature relativistic framework, Eur. Phys. J. A **55**, 223 (2019).

[30] H. Wibowo and E. Litvinova, Nuclear dipole response in the finite-temperature relativistic time-blocking approximation, Phys. Rev. C **100**, 024307 (2019).

[31] N. D. Dang and A. Arima, Quantal and Thermal Dampings of Giant Dipole Resonances in ^{90}Zr, ^{120}Sn, and ^{208}Pb, Phys. Rev. Lett. **80**, 4145 (1998).

[32] N. Dinh Dang and A. Arima, Phonon damping model using random-phase-approximation operators, Phys. Rev. C **64**, 024302 (2001).

[33] N. Dinh Dang and A. Arima, Temperature dependence of quantal and thermal dampings of the hot giant dipole resonance, Nucl. Phys. A **636**, 427 (1998).

[34] N. Dinh Dang, Damping of giant dipole resonances in hot rotating nuclei, Phys. Rev. C **85**, 064323 (2012).

[35] M. Gallardo, M. Diebel, T. Døssing, and R. Broglia, Damping of the giant dipole resonance in hot, strongly rotating nuclei, Nucl. Phys. A **443**, 415 (1985).

[36] D. Kusnezov, Y. Alhassid, and K. A. Snover, Scaling Properties of the Giant Dipole Resonance Width in Hot Rotating Nuclei, Phys. Rev. Lett. **81**, 542 (1998).

[37] A. Ansari, N. Dinh Dang, and A. Arima, Thermal shape and orientation fluctuation corrections for the hot giant dipole resonance within the static path approximation, Phys. Rev. C **63**, 024310 (2001).

[38] Y. Alhassid, B. Bush, and S. Levit, Thermal Shape Fluctuations, Landau Theory, and Giant Dipole Resonances in Hot Rotating Nuclei, Phys. Rev. Lett. **61**, 1926 (1988).

[39] A. K. Rhine Kumar and P. Arumugam, Thermal shape fluctuation model study of the giant dipole resonance in ^{152}Gd, Phys. Rev. C **92**, 044314 (2015).

[40] W. E. Ormand, P. F. Bortignon, and R. A. Broglia, Temperature Dependence of the Width of the Giant Dipole Resonance in ^{120}Sn and ^{208}Pb, Phys. Rev. Lett. **77**, 607 (1996).

[41] Y. Alhassid and B. Bush, Effects of orientation fluctuations on the angular distribution of the giant dipole resonance γ-rays in hot rotating nuclei, Nucl. Phys. A **531**, 39 (1991).

[42] Y. Alhassid, B. Bush, and S. Levit, Landau theory of shapes, shape fluctuations and giant dipole resonances in hot nuclei, Nucl. Phys. A **482**, 57 (1988).

[43] Y. Alhassid and B. Bush, Effects of thermal fluctuations on giant dipole resonances in hot rotating nuclei, Nucl. Phys. A **509**, 461 (1990).

[44] J. Gaardhøje, A. Atac, A. Maj, A. Bracco, F. Camera, B. Million, M. Pignanelli, and E. Rebesco, Gamma decay of giant dipole resonances and the shapes and fluctuations of hot nuclei, Nucl. Phys. A **538**, 573 (1992).

[45] A. L. Goodman, Thermal shape fluctuations in hot rotating nuclei: Comparison of constant energy constraint and constant temperature constraint, Nucl. Phys. A **528**, 348 (1991).

[46] A. K. Rhine Kumar, P. Arumugam, and N. D. Dang, Pairing effect in the thermal shape-fluctuation model on the width of the giant dipole resonance, Phys. Rev. C **90**, 044308 (2014).

[47] A. K. Rhine Kumar, P. Arumugam, and N. D. Dang, Effects of thermal shape fluctuations and pairing fluctuations on the giant dipole resonance in warm nuclei, Phys. Rev. C **91**, 044305 (2015).

[48] P. Ring and P. Schuck, *The Nuclear Many-Body Problem* (Springer-Verlag, New York, 1980).

[49] D. Pandit, S. Mukhopadhyay, S. Pal, A. De, and S. Banerjee, Critical behavior in the variation of GDR width at low temperature, Phys. Lett. B **713**, 434 (2012).

[50] A. Ansari, N. Dinh Dang, and A. Arima, Hot giant dipole resonance with thermal shape fluctuation corrections in the static path approximation, Phys. Rev. C **62**, 011302(R) (2000).

[51] Y. Alhassid, Giant dipole resonances in hot rotating nuclei: Overview and recent advances, Nucl. Phys. A **649**, 107 (1999).

[52] A. L. Goodman, Thermal shape fluctuations at constant energy, Nucl. Phys. A **520**, c567 (1990).

[53] A. L. Goodman, Finite-temperature HFB theory, Nucl. Phys. A **352**, 30 (1981).

[54] J. C. Pei, W. Nazarewicz, J. A. Sheikh, and A. K. Kerman, Fission Barriers of Compound Superheavy Nuclei, Phys. Rev. Lett. **102**, 192501 (2009).

[55] F. A. Dodaro and A. L. Goodman, Statistical orientation fluctuations in ^{188}Os, Nucl. Phys. A **596**, 91 (1996).

[56] J. Sadhukhan, J. Dobaczewski, W. Nazarewicz, J. A. Sheikh, and A. Baran, Pairing-induced speedup of nuclear spontaneous fission, Phys. Rev. C **90**, 061304(R) (2014).

[57] A. Baran, J. A. Sheikh, J. Dobaczewski, W. Nazarewicz, and A. Staszczak, Quadrupole collective inertia in nuclear fission: Cranking approximation, Phys. Rev. C **84**, 054321 (2011).

[58] V. Martin, J. L. Egido, and L. M. Robledo, Thermal shape fluctuation effects in the description of hot nuclei, Phys. Rev. C **68**, 034327 (2003).

[59] J. Bartel, P. Quentin, M. Brack, C. Guet, and H.-B. Håkansson, Towards a better parametrisation of Skyrme-like effective forces: A critical study of the SkM force, Nucl. Phys. A **386**, 79 (1982).

[60] E. Chabanat, P. Bonche, P. Haensel, J. Meyer, and R. Schaeffer, A Skyrme parametrization from subnuclear to neutron star densities Part II. Nuclei far from stabilities, Nucl. Phys. A **635**, 231 (1998).

[61] J. Dobaczewski, W. Nazarewicz, and M. V. Stoitsov, Nuclear ground-state properties from mean-field calculations, Eur. Phys. J. A **15**, 21 (2002).

[62] J. Dobaczewski and P. Olbratowski, Solution of the Skyrme–Hartree–Fock–Bogolyubov equations in the Cartesian deformed harmonic-oscillator basis. (IV) HFODD (v2.08i): a new version of the program, Comput. Phys. Commun. **158**, 158 (2004).

[63] N. Schunck, J. Dobaczewski, J. McDonnell, W. Satuła, J. Sheikh, A. Staszczak, M. Stoitsov, and P. Toivanen, Solution of the Skyrme–Hartree–Fock-Bogolyubov equations in the Cartesian deformed harmonic-oscillator basis.: (VII) HFODD (v2.49t): A new version of the program, Comput. Phys. Commun. **183**, 166 (2012).

[64] N. Dinh Dang, M. Ciemala, M. Kmiecik, and A. Maj, Giant dipole resonance in ^{88}Mo from phonon damping model strength functions averaged over temperature and angular momentum distributions, Phys. Rev. C **87**, 054313 (2013).

[65] A. Bohr and B. Mottelson, *Nuclear Structure, Vol. II* (W.A. Benjamin, New York, 1975).

[66] B. Bush and Y. Alhassid, On the width of the giant dipole resonance in deformed nuclei, Nucl. Phys. A **531**, 27 (1991).

[67] D. L. Hill and J. A. Wheeler, Nuclear constitution and the interpretation of fission phenomena, Phys. Rev. **89**, 1102 (1953).

[68] W. J. Knox, A. R. Quinton, and C. E. Anderson, Evaporation of charged particles from highly excited compound nuclei, Phys. Rev. **120**, 2120 (1960).

[69] V. Kolomietz, Splashing and evaporation of nucleons from excited nuclei, Nucl. Phys. A **743**, 211 (2004).

[70] O. Wieland, A. Bracco, F. Camera, G. Benzoni, N. Blasi, S. Brambilla, F. Crespi, A. Giussani, S. Leoni, P . Mason, B. Million, A. Moroni, S. Barlini, V. L. Kravchuk, F. Gramegna, A. Lanchais, P. Mastinu, A. Maj, M. Brekiesz, M. Kmiecik, M. Bruno, E. Geraci, G. Vannini, G. Casini, M. Chiari, A. Nannini, A. Ordine, and E. Ormand, Giant Dipole Resonance in the Hot and Thermalized ^{132}Ce Nucleus: Damping of Collective Modes at Finite Temperature, Phys. Rev. Lett. **97**, 012501 (2006).

[71] D. Santonocito and Y. Blumenfeld, The hot GDR revisited, Eur. Phys. J. A **56**, 279 (2020).

[72] P. Fröbrich and I. Gontchar, Langevin description of fusion, deep-inelastic collisions and heavy-ion-induced fission, Phys. Rep. **292**, 131 (1998).

[73] N. D. Dang and A. Arima, Pairing effect on the giant dipole resonance width at low temperature, Phys. Rev. C **68**, 044303 (2003).

[74] E. Ramakrishnan, T. Baumann, A. Azhari, R. A. Kryger, R. Pfaff, M. Thoennessen, S. Yokoyama, J. R. Beene, M. L. Halbert, P. E. Mueller, D. W. Stracener, R. L. Varner, R. J. Charity, J. F. Dempsey, D. G. Sarantites, and L. G. Sobotka, Giant Dipole Resonance Built on Highly Excited States of ^{120}Sn Nuclei Populated by Inelastic α Scattering, Phys. Rev. Lett. **76**, 2025 (1996).

[75] A. Bracco, F. Camera, O. Wieland, and W. E. Ormand, Progress in the study of the γ-decay of the giant dipole resonance in hot nuclei, Mod. Phys. Lett. A **22**, 2479 (2007).

[76] N. Schunck, D. Duke, H. Carr, and A. Knoll, Description of induced nuclear fission with Skyrme energy functionals: Static potential energy surfaces and fission fragment properties, Phys. Rev. C **90**, 054305 (2014).